Phase Behavior of Aqueous Poly(ethylene oxide)/Poly(propylene oxide) Solutions

M. Malmsten,*,† P. Linse,‡ and K.-W. Zhang‡

Astra Arcus AB, S-151 85 Södertälje, Sweden, and Physical Chemistry 1, Chemical Center, University of Lund, P.O. Box 124, S-221 00 Lund, Sweden

Received October 22, 1992; Revised Manuscript Received February 8, 1993

ABSTRACT: The phase behavior of aqueous solutions of poly(ethylene oxide) (PEO) and poly(propylene oxide) (PPO) has been investigated. Experimentally, it was observed that the ternary phase diagram displays a closed immiscibility region. At 25 °C, the tie lines indicate that each phase is enriched in one of the polymers. Furthermore, the water content is higher in the PEO-enriched phase. Increasing the temperature, i.e., worsening the solvency for both PPO and PEO, results in a growth of the immiscibility region. Furthermore, the relative water content in the PPO-enriched phase decreases, whereas PEO distributes more evenly between the phases. A good agreement was found between the experimental findings and results from model calculations using a mean-field theory for polymers possessing internal states. Furthermore, details about the state distributions of PEO and PPO are discussed.

Introduction

It is generally observed that, in a ternary phase diagram of two polymers and one solvent, there is a two-phase region.[1] This effect is referred to as polymer incompatibility (aggregative phase separation is not included in the present discussion) and is of both fundamental interest and technical importance. For example, it has been found that such two-phase polymer systems can be utilized in both large- and small-scale biotechnical separations, such as protein purification.[2]

The origin of polymer incompatibility is an effectively repulsive polymer–polymer interaction. Due to the connectivity of polymers, the entropy loss per segment on phase separation is small, and, especially for high molecular weight polymers, a very small unfavorable polymer–polymer interaction energy is sufficient to cause phase separation. This explains the observation that if two polymers are incompatabile in one solvent, they are often incompatible in other solvents as well.

There is also, however, a slightly different phase-separation mechanism. This originates from differences in the polymer–solvent interactions. Thus, even if the interaction between polymer 1 and polymer 2 is athermal ($\chi_{12} = 0$, χ being defined as a Flory–Huggins parameter[1]), phase separation is possible, provided that the polymer–solvent interaction parameters are different ($\chi_{2s} \neq \chi_{1s}$).[3-5] The phase diagram of such a system is expected to be different from those originating from an effectively unfavorable polymer–polymer interaction ($\chi_{12} > 0$). While the two-phase region is "parabolic" in the latter case, one expects to find a closed immiscibility region in the former, since no phase separation occurs at low solvent contents.

In this context, a system which could be expected to display a closed-loop phase behavior is the PEO/PPO/water system [PEO and PPO being poly(ethylene oxide) and poly(propylene oxide), respectively]. The reason for this is that, due to their structural similarity, PEO and PPO are expected to form close to athermal binary mixtures. However, PPO interacts much more unfavorably with water.[6]

Both PEO and PPO display a reversed temperature-dependent phase behavior in water, manifested by a lower consolute temperature. Thus, aqueous solutions of PEO and PPO are one-phase systems at low temperatures, whereas a phase separation occurs on increasing the temperature.[6] Although this reversed temperature dependence is well-known both for nonionic surfactants and polymers, the mechanisms are still under debate.[7] Several models have been developed, focusing on either water structure,[8,9] hydrogen bonding,[10,11] or conformational effects.[12]

Ourselves, we have focused on temperature-dependent conformational effects.[12] From quantum mechanical calculations,[13] the conformations of EO segments are divided into two classes, one being polar, having a low energy but a low statistical weight, and one being less polar, or nonpolar, having a higher energy but a higher statistical weight. (This subdivision is furthermore consistent with ^{13}C-NMR chemical shift measurements.[14]) At low temperatures, the former class of states dominates and the polymer–water interaction is favorable, whereas at higher temperatures, the latter states become increasingly populated, rendering the polymer–water interaction less favorable. Furthermore, the state distribution depends on the polymer concentration; the fraction of polar states decreases with an increasing polymer concentration.

The Flory–Huggins polymer theory extended with internal states for describing the reverse temperature dependence has previously been used successfully for modeling the phase behavior of the PEO/water[12] and the PPO/water[15] binary systems, as well as that of the PEO/dextran/water system.[16] Moreover, an extended model for heterogeneous systems of polymers possessing internal states has been used successfully in modeling the temperature-dependent micellization of PEO/PPO/PEO block copolymers[17] and the adsorption properties of these polymers,[18,19] as well as protein partitioning in the PEO/dextran/water and UCON/dextran/water systems (UCON being a random copolymer of EO and PO).[20]

Considering the possible occurrence of a closed immiscibility region in the PEO/PPO/water system, we decided to investigate this system and to see whether the model was capable of reproducing and explaining the experimental findings, and in particular the temperature dependence of the phase behavior. The study is furthermore expected to be of interest for the understanding of PEO/PPO/PEO block copolymers, which are now widely used

† Astra Arcus AB. Present address: Institute for Surface Chemistry, P.O. Box 5607, S-11486 Stockholm, Sweden.
‡ University of Lund.

0024-9297/93/2226-2905$04.00/0

for both fundamental investigations and practical applications.

Experimental Section

Materials. Poly(ethylene oxide) and poly(propylene oxide) of molecular weights 600 and 400, respectively (polydispersity unknown), were obtained from Fluka, Germany. [The reason for choosing to work with such short polymers (oligomers) is that PPO of higher molecular weight is only very sparingly soluble in water at room temperature. In order to get reasonably symmetric phase diagrams, we further chose a PEO of a comparable molecular weight.] The lower consolute temperature (LCT) for PPO 400 is 53 °C (results not shown), while that of PEO 600 is well above 150 °C.[21] D_2O was obtained from Norsk Hydro, Norway.

Methodology. The PEO/PPO/water phase diagrams were obtained by weighing the components, mixing them together, and leaving the samples for equilibration at either 25 or 53 °C for a few days. (Between 150 and 250 samples were prepared for each phase diagram.) Due to the low molecular weights and the low viscosities, this was more than ample time for equilibration. (The uncertainty in the temperature is about ±1–2 °C. In fact, the finding that the two-phase boundary coincides with the PPO–water binary line at the higher temperature seems to indicate that the actual temperature in this case is slightly higher than the LCT of PPO). The tie lines were obtained from ^{1}H-NMR spectra (i.e., methyl and methylene resonance intensities) for the separate phases after several weeks of equilibration. For calibration purposes, 1.0% sodium acetate was added to the samples. Furthermore, D_2O was added to suppress the strong water peak and thereby achieve a better estimate of the PEO and PPO concentrations, especially at higher water content. The spectrometer used was a Jeol FX-60 operating at 60 MHz.

Model Calculations

The Flory–Huggins lattice theory for homogeneous polymer solutions has been extended to describe polymers possessing internal degrees of freedom.[12] This extension provides a means of modeling effective segment–segment interaction parameters which are temperature as well as concentration dependent. The basis of the model is that the distribution of conformations of a segment depends on temperature and that different conformations interact differently with adjacent polymer segments and solvent molecules. The conformations of the OCCO segment of PEO are divided into two classes or states, one being polar and having a low energy but a low statistical weight and one being less polar, or nonpolar, having a higher energy but a higher statistical weight. At low temperature the former state is dominating, and thus a more favorable polymer–water interaction is obtained, whereas at elevated temperatures, the latter state becomes progressively more important, resulting in a more unfavorable polymer–water interaction.

The basis of the phase diagram calculation is the expression for the mixing free energy. For a multicomponent system consisting of solvent(s) and polymer(s) with internal states, the Helmholtz free energy of mixing becomes[15]

$$\beta(A - A^*) = \beta(A_{int} - A_{int}^*) - \ln\frac{\Omega}{\Omega^*} + \beta(U - U^*) \quad (1)$$

where A_{int} represents the internal energy in the mixed system, A_{int}^* is the internal energy in the reference system (where the components are in pure amorphous states), $\ln(\Omega/\Omega^*)$ is the mixing configurational entropy divided by the Boltzmann constant, U and U^* are the configurational energy in the mixed and reference systems, respectively, and $\beta = 1/(kT)$, k being the Boltzmann constant and T the temperature. For the general case of a system with copolymers, the internal free energy, the mixing configurational entropy, and the interaction energy are given by[15]

$$\beta A_{int} = \sum_x \sum_A n_x r_{Ax} \sum_B P_{AB}\left[\beta U_{AB} + \ln\frac{P_{AB}}{g_{AB}}\right] \ln\frac{\Omega}{\Omega^*} = -\sum_x n_x \ln\frac{n_x r_x}{L}\beta U = \frac{1}{2}\sum_x \sum_A \sum_{A'} \sum_B \sum_{B'} n_x r_{Ax} P_{AB} \chi_{BB'} \times P_{A'B'}\phi_{A'} \quad (2)$$

where r_{Ax} denotes the number of segments of type A in component x, r_x the total number of segments in component x ($r_x = \sum_A r_{Ax}$), n_x the total number of molecules of type x, L the total number of lattice sites ($L = \sum_x n_x r_x$), ϕ_A the volume fraction of species A [$\phi_A = (1/L)\sum_x n_x r_{Ax}$], and $\chi_{BB'}$ the Flory–Huggins interaction parameter between species A in state B and species A′ in state B′. Moreover, P_{AB} is the fraction of species A in state B, U_{AB} the zero energy level of species A in state B, and g_{AB} the degeneration of species A in state B.

From the free energy of mixing, the chemical potential of component x can be derived according to $\mu_x - \mu^*_x = \partial(A - A^*)/\partial n_x$, giving

$$\beta(\mu_x - \mu^*_x) = r_x \sum_A \sum_B \phi^*_{Ax}\left\{P_{AB}\left[\beta U_{AB} + \ln\frac{P_{AB}}{g_{AB}}\right] - P^*_{AB}\left[\beta U_{AB} + \ln\frac{P^*_{AB}}{g^*_{AB}}\right]\right\} + \ln\phi_x + 1 - r_x\sum_{x'}\frac{\phi_{x'}}{r_{x'}} - \frac{r_x}{2}\sum_A \sum_{A'} \sum_B \sum_{B'}[(\phi_{A'} - \phi^*_{Ax})P_{AB}\chi_{BB'}P_{A'B'}(\phi_{A'} - \phi^*_{A'x}) + \phi^*_{Ax}\phi^*_{A'x}\chi_{BB'}(P^*_{AB}P^*_{A'B'} - P_{AB}P_{A'B'})] \quad (3)$$

where an asterisk denotes quantities in the reference state. In particular, ϕ^*_{Ax} denotes the volume fraction of species A in pure component x ($\phi^*_{Ax} = r_{Ax}/r_x$). The fraction of species A being in state B at equilibrium is obtained by minimizing A with respect to $\{P_{AB}\}$ subjected to the constraint $\sum_B P_{AB} = 1$, for all A, which gives

$$P_{AB} = \frac{X_{AB}}{\sum_B X_{AB}}, \qquad X_{AB} \equiv g_{AB}\exp[-\beta U_{AB} - \sum_{A'}\sum_{B'}\chi_{BB'}P_{A'B'}\phi_{A'}] \quad (4)$$

In the case of homopolymers with no internal degrees of freedom, eq 3 reduces to

$$\beta(\mu_x - \mu^*_x) = \ln\phi_x + 1 - r_x\sum_{x'}\frac{\phi_{x'}}{r_{x'}} + r_x[(1 - \phi_x)\sum_{x'}\chi_{xx'}\phi_{x'} - \sum_{x'<x''}\phi_{x'}\chi_{x'x''}\phi_{x''}] \quad (5)$$

which, for the special case of a three-component system consisting of one polymer and two solvents, agrees with the expressions given by Scott.[22]

Given the overall composition of the system $\{n_x\}$, equilibrium is achieved when $\{n_x\}$ is distributed among the coexisting phases $\{\alpha\}$ such that the total free energy $A^{tot} = \sum_\alpha A^\alpha(\{n_x^\alpha\})$, where $A^\alpha(\{n_x^\alpha\})$ is given by eqs 1 and 2, attains its global minimum, or equivalently, when the chemical potential of each component given by eq 3 is the same in all coexisting phases.

Since aqueous solutions of both PEO and PPO display lower consolute points,[6] both EO and PO segments are

Table I. Internal State Parameters U_{AB} (Energy) and g_{AB} (Statistical Weight) and Flory–Huggins Interaction Parameters ($\chi_{BB'}$) for the PEO/PPO/Water System (Energy in kJ/mol)

species	state	state no.	U_{AB}	g_{AB}
water		1	0	1
EO	polar	2	0[a]	1[a]
	nonpolar	3	5.086[a]	8[a]
PO	polar	4	0[b]	1[b]
	nonpolar	5	11.5[b]	60[b]

$kT\chi_{BB'}$

	state no.			
state no.	2	3	4	5
1	0.6508[a]	5.568[a]	1.7[b]	8.5[b]
2		1.266[a]	1.8	3.0
3			0.5	−2.0
4				1.4[b]

[a] From fit to the experimental PEO/water phase diagram.[12] See also ref 23. In the original work,[12] the energy parameters were given to four figures, of which probably two are significant. In order to be consistent with this work,[12] we have refrained from truncating these parameters. [b] From fit to the experimental PPO/water phase diagram.[15]

modeled with two internal states, one polar and one nonpolar. The parameters describing the internal degrees of freedom of PEO as well as the EO–water interaction parameters (given in Table I) were previously obtained by fitting the theoretical PEO–water phase diagram to the experimental one.[12,23] The same procedure was used for the corresponding PPO and PO–water parameters.[15] It should be noticed that the parameters fitted correspond to clear physical properties.

In order to be able to perform the model calculations of the PEO/PPO/water phase diagram, we also require parameters for the EO–PO interaction (Table I). In the present study these were obtained by fitting the calculated ternary phase diagram to the experimental one at the two temperatures. It should be mentioned that, in previous modeling of EO and PO containing systems,[17–19] a different set of EO–PO interaction parameters was used. In the previous studies, the effect of these parameters on the results was limited due to the small polymer concentration, and thus the ad hoc procedure of assigning values to these parameters was acceptable.

Although the interaction parameters are assigned to pairs of segments in different states, it is fruitful to consider averaged segment–segment interaction parameters, $\chi_{AA'}$. These are obtained by averaging $\chi_{BB'}$ over all pairs of internal states according to

$$\chi_{AA'} = \sum_{B}\sum_{B'} P_{AB}P_{A'B'}\chi_{BB'} \qquad (6)$$

Although $\chi_{BB'}$ is fixed, the averaged segment–segment interaction parameter is temperature as well as composition dependent, since the fraction of species being in different states depends on temperature and composition (cf. eq 4).

Results and Discussion

As is shown in Figures 1 and 2, the PEO/PPO/water system displays a closed immiscibility region. At high water content, the system forms a one-phase system, irrespective of the PEO/PPO ratio. The very high total polymer concentration needed to induce phase separation ($c_{crit} \approx 50$ wt% at 25 °C) is most likely due to the very low molecular weight of the polymers.[1] Also at very low water content, the system shows a one-phase region over the entire PEO/PPO composition range, which indicates that the interaction between PEO and PPO is close to athermal in the absence of water. At intermediate water concentrations (≈15–50 wt % water), however, an immiscibility region is observed. Clearly, the phase separation is related to the polymer–water interactions.

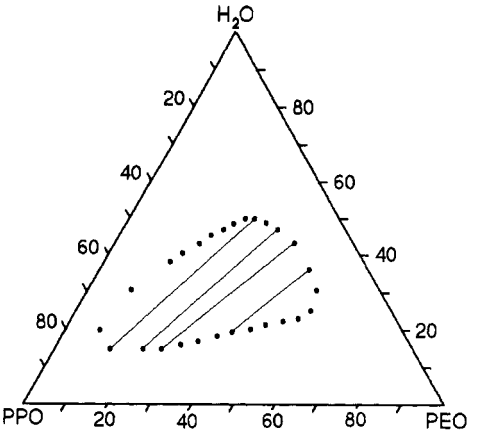

Figure 1. Experimental phase diagram for the PEO 600/PPO 400/water system at 25 °C.

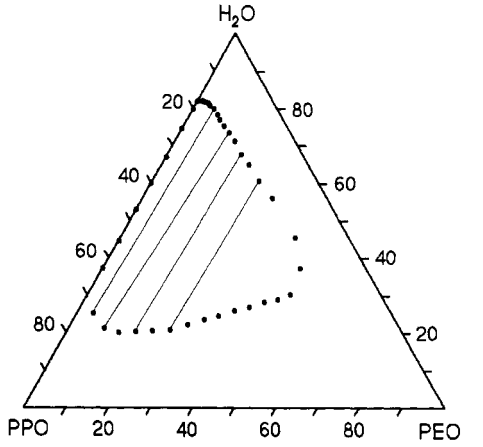

Figure 2. Experimental phase diagram for the PEO 600/PPO 400/water system at 53 °C.

As can be seen in Figure 1, the tie lines at 25 °C indicate that each phase is enriched in one of the polymers, as would be expected from the previous discussion. Furthermore, the PEO-enriched phase has a higher water content that the PPO-enriched phase. Again, this is what one would expect, since the solvency conditions for PPO are worse than those for PEO (cf. LCT's).

Although the influence of the solvent on the ternary phase behavior has been known theoretically for quite some time,[3–5] only sparse experimental data are available on these effects. However, Hugelin and Dondos,[24] as well as Kern,[25] showed that an asymmetry in the polymer–solvent interaction parameters increases the polymer incompabitility. Furthermore, Bank et al.[26] observed that polystyrene is compatible with poly(vinyl methyl ether) in toluene, benzene, and perchloroethylene but incompatible in chloroform, methylene chloride, and trichloroethylene. Moreover, a closed-loop phase behavior has been reported for several systems, including the diphenyl ether/polyethylene/atactic polypropylene system[27] and for polystyrene/poly(vinyl methyl ether) in chloroform, trichloroethene, and dichloromethane.[5,28,29] A closed-loop phase diagram has further been observed for an aqueous system containing poly(ethylene oxide) and a nonionic surfactant (C_4E_1), although the interpretation of the latter finding is somewhat complicated, due to the complexity of the system.[30]

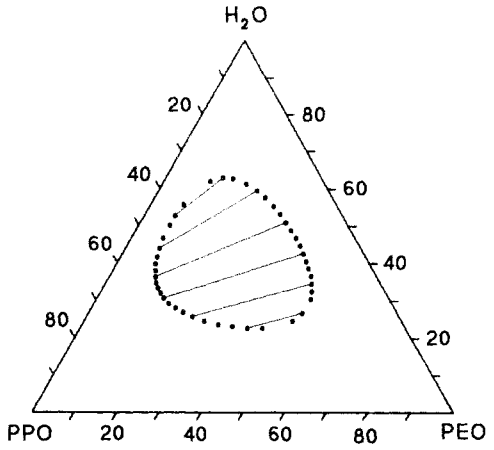

Figure 3. Calculated phase diagram for the $(EO)_{14}/(PO)_7$/water system at 25 °C.

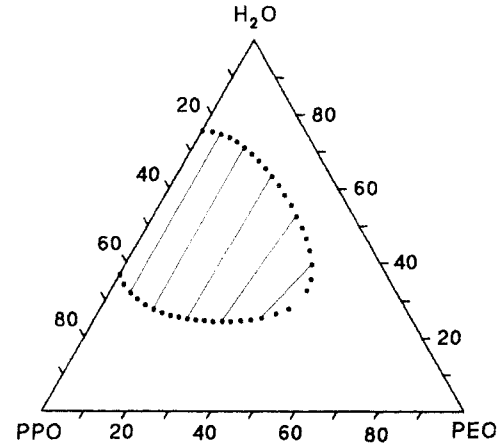

Figure 4. Calculated phase diagram for the $(EO)_{14}/(PO)_7$/water system at 53 °C.

On increasing the temperature, both the EO–water and the PO–water interactions become more unfavorable. Model calculations show that the *changes* in $kT\chi_{water,EO}$ and $kT\chi_{water,PO}$ are similar, viz. 0.2 kJ/mol in the water corner and 0.7–0.8 kJ/mol for an equal mixture of EO and PPO on increasing the temperature from 25 to 53 °C. The increase of the water–polymer interaction parameters is expected to contribute to an increase in the extension of the two-phase region.[3-5] The strongest increase in the immisicibility region occurs toward the PPO–water binary line. (The finding that the two-phase region reaches the PPO–water binary line seems to indicate that the actual temperature is slightly higher than the LCT for PPO in the latter case.) Furthermore, with increasing temperature, the distribution of water becomes more uneven; i.e., at higher temperature, the PPO-enriched phase is further depleted in water. Again, this is what one would expect, considering the poor solvency conditions for PPO at 53 °C. A similar temperature dependence has previously been observed for the PEO/dextran/water system, where it was found that on approaching the LCT for PEO, the water is distributed toward the dextran-enriched phase to an increasing extent.[16] Interestingly, PEO distributed rather evenly between the phases at 53 °C, which means that, at this temperature, the phase separation is primarily driven by the unfavorable PO–water interaction.

As can be seen in Figures 3 and 4, model calculations with the mean-field lattice theory for polymers possessing internal states are quite capable of reproducing the experimental findings. Thus, at the lower temperature a closed-loop immiscibility region is found at intermediate water content. Furthermore, each phase is enriched in one of the polymers, and the water is somewhat unevenly distributed toward the PEO-enriched phase. Increasing the temperature to 53 °C results in a growth of the two-phase region, in particular toward the PPO–water binary line. Furthermore, the water distribution becomes more uneven at the higher temperature.

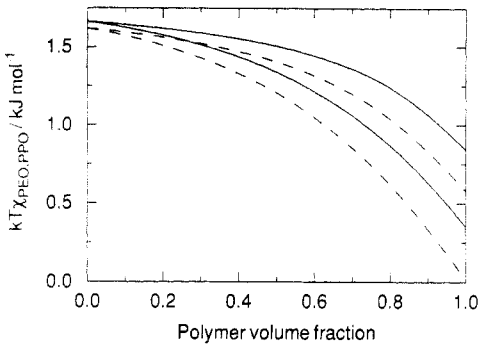

Figure 5. Averaged interaction parameter between PEO and PPO ($kT\chi_{EO,PO}$) versus the total polymer volume fraction at 25 °C (solid curves) and 53 °C (dashed curves). The PEO/PPO ratio was 100/0 (top) and 0/100 (bottom).

In the model calculations, the parameters describing the internal PEO and PPO, as well as the EO–water and PO–water interactions, were taken from previous fits to the PEO/water and the PPO/water phase diagrams, respectively. Furthermore, the experimental data of the PEO/PPO/water phase diagrams (Figures 1 and 2) were used to fit the EO–PO interaction parameters. Although the number of fitted EO–PO interaction parameters may be considered as large, viz., four ($\chi_{EO,polar;PO,polar}$, $\chi_{EO,polar;PO,nonpolar}$, $\chi_{EO,nonpolar;PO,polar}$, and $\chi_{EO,nonpolar;PO,nonpolar}$), the requirement of obtaining acceptable extensions of the two-phase regions and slopes of the tie lines, and at two different temperatures with different phase behavior, puts a large restriction on the acceptable subspace of the four state–state interaction parameters. The uncertainty in the values reported (Table I) is of the order 0.2 kJ/mol, except for the nonpolar–nonpolar interaction, where it is about 0.5 kJ/mol. The reason for the larger uncertainty in the latter case is the comparably small fraction of nonpolar states. The values obtained seem reasonable. For example, the largest repulsion (3.0 kJ/mol) appears between EO segments in the polar state and PO segments in the nonpolar state, whereas the least repulsive component of the averaged EO–PO interaction arises from the nonpolar–nonpolar interaction. The reason for $\chi_{EO,nonpolar;PO,nonpolar}$ being negative, and not slightly positive as might have been expected, is probably to be found in the simplicity of the model, rather than in any specific molecular mechanism.

Within the model, the origin of the phase separation is to be found in the conformational adaptation. Since the distribution of conformational states vary with temperature and concentration and since different conformational states interact differently both with water and among each other, the averaged polymer–polymer and polymer–water interactions will vary within the ternary phase diagram. This is partly illustrated in Figure 5, showing the averaged PEO–PPO interaction parameter, evaluated according to eq 6, as a function of temperature, water content, and composition of the polymer mixture. As can be seen, $kT\chi_{EO,PO}$ decreases with increasing polymer volume fraction. The reason for this is that, with an increasing total polymer volume fraction, the fraction of polar states of both PEO and PPO decreases. Since the EO–PO interaction is most favorable when these are in their unpolar states, the averaged interaction parameter $kT\chi_{EO,PO}$

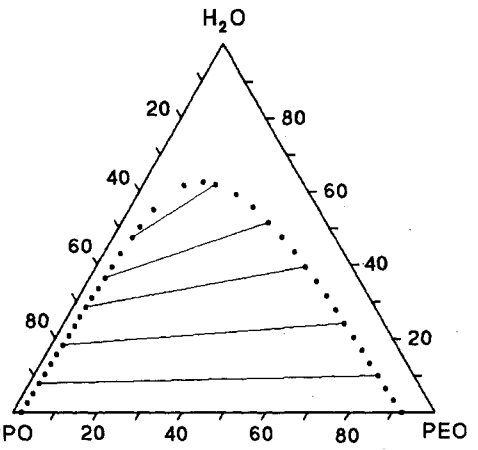

Figure 6. Calculated phase diagram for the $(EO)_{14}/(PO)_7$/water system at 25 °C. The value of $kT\chi_{EO,PO}$ was 1.50 kJ/mol throughout the phase diagram.

decreases with increasing the total polymer volume fraction. Furthermore, the fraction of polar states decreases with increasing temperature, as well as with an increasing PPO fraction, rendering $kT\chi_{EO,PO}$ lower at a higher temperature and a higher PPO content, respectively (Figure 5). More specifically, at 25 °C and a PEO/PPO ratio of 50/50, $kT\chi_{EO/PO}$ equals 0.41, 1.0, and 1.5 kJ/mol at a water volume fraction of 0 (binary PEO–PPO line), 0.22 (lower water limit of the two-phase region), and 0.62 (upper water limit of the two-phase region), respectively. At 53 °C, the values are 0.11, 0.85, and 1.45 kJ/mol at water volume fractions of 0 (binary PEO–PPO line), 0.25 (lower water limit of the two-phase region), and 0.68 (upper water limit of the two-phase region), respectively. The necessity of having a temperature- as well as concentration-dependent $\chi_{EO,PO}$ can be illustrated by calculating the phase diagram with fixed values of $\chi_{EO,PO}$. At a value of $kT\chi_{EO,PO}$ of 1.5 kJ/mol at 25 °C (corresponding to the upper water limit of the two-phase region), a traditional incompatibility system is obtained, displaying a parabolic two-phase region between about 2% and 92% PEO and with a critical point at a water content of about 65% (Figure 6). If instead $kT\chi_{EO,PO}$ is chosen as 0.41 kJ/mol (corresponding to the binary PEO–PPO system) or 1.0 kJ/mol (corresponding to the lower water limit of the two-phase region), no phase separation is obtained at 25 °C.

The behavior at 53 °C is richer. On initially increasing the value of $\chi_{EO,PO}$ from athermal ($kT\chi_{EO,PO} = 0$), the two-phase region decreases. At about $kT\chi_{EO,PO} = 0.85$ kJ/mol (corresponding to the lower water limit of the two-phase region; cf. Figure 4), the extension of the two-phase region has its minimum. At even larger values of the averaged EO–PO interaction parameter, the PPO–water two-phase region increases again and finally joins the growing PEO–PPO incompatibility two-phase region (Figure 7). At $kT\chi_{EO,PO} = 1.45$ kJ/mol (corresponding to the upper water limit of the two-phase region; cf. Figure 4), a large two-phase region, extending from the PEO–PPO binary line to the PPO–water binary line, is obtained.

The decrease and then increase of the two-phase region on increasing $\chi_{EO,PO}$ is a consequence of a delicate balance of the free energy of a system of a given composition and of possible phase-separated systems. Consider a system with a composition corresponding to the two-phase region close to the critical point of the phase diagram obtained with $kT\chi_{EO,PO} = 0.11$ kJ/mol (Figure 7a). The phase separation shown in Figure 7a causes the number of PEO–PPO contacts to *increase* (cf. tie lines). At larger values $\chi_{EO,PO}$ this increase in the number of contacts becomes

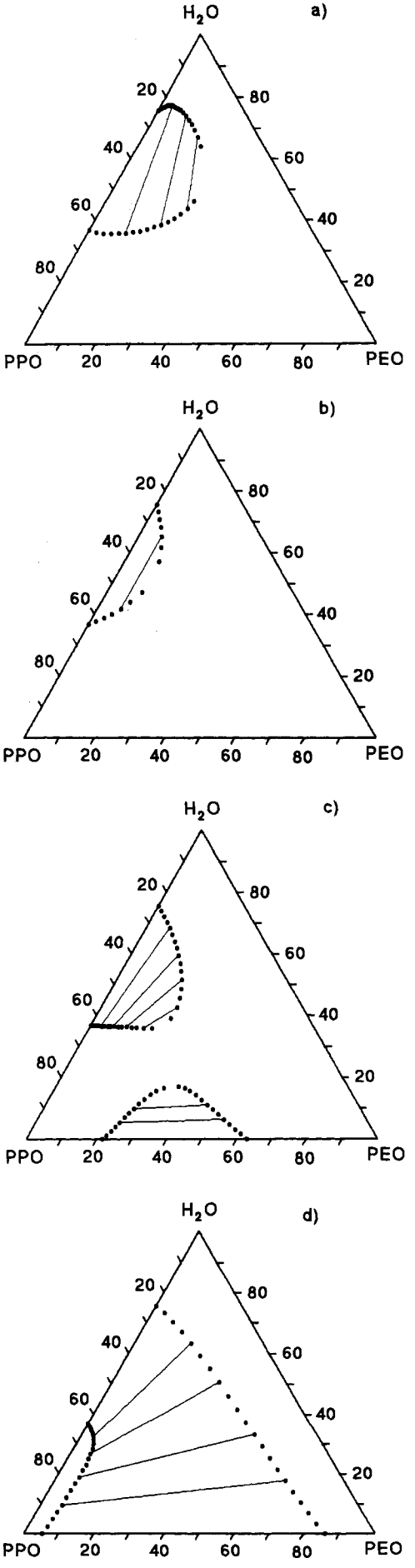

Figure 7. Calculated phase diagram for the $(EO)_{14}/(PO)_7$/water system at 53 °C. The values of $kT\chi_{EO,PO}$ were (a) 0.11, (b) 0.85, (c) 1.26, and (d) 1.45 kJ/mol throughout each phase diagram.

more costly, and at some $\chi_{EO,PO}$ the free energy of two separated phases combined exceeds that of the single phase and hence no phase separation occurs. At even higher values of $\chi_{EO,PO}$, the system can again gain free energy by phase separation, but now the composition of the separated phases differs from those for small values of $\chi_{EO,PO}$. In fact, the tie lines show that the number of PEO–PPO contacts *decreases* on phase separation. This behavior is *not* a direct consequence of the conformational adaptation. On the contrary, the state distribution is invariant for changes in $\chi_{EO,PO}$ (cf. eq 4).

Previously, it has been shown that, in order to describe the existence of a LCT in the PEO/water and the PPO/water binary phase diagrams within the framework of the Flory–Huggins theory, a temperature-dependent averaged polymer–water interaction parameter is required. For describing the PEO/PPO/water phase diagram, which displays several unusual features, it appears from the present investigation that also composition-dependent interaction parameters are necessary. The two-state model of PEO and PPO offers a possibility of including both these dependencies in a uniform way. Given the good agreement between the experimental and calculated phase diagrams, the EO–PO interaction parameters are now more satisfactorily determined and the predictive capacity of the model may be assessed in further investigations at high PEO and PPO volume fractions.

Summary

The phase behavior of the ternary PEO 600/PPO 400/water system has been investigated. It was found that this system displays a closed immiscibility loop. At 25 °C, the tie lines indicate that each phase is enriched in one of the polymers and that the water is somewhat unevenly distributed toward the PEO-enriched phase. On increasing the temperature to slightly above the LCT for PPO, the extent of the immiscibility region increases and reaches the PPO–water binary line. Furthermore, the relative water content of the PPO-enriched phase decreases, while PEO distributes more evenly between the phases. Model calculations, taking into account the temperature and density dependence of the system by accounting for internal states, are in good agreement with the experimental findings.

Acknowledgment. Ingegerd Lind is gratefully acknowledged for experimental help. This work was financed by the Swedish National Board for Technical Development (STU/NUTEK) and the Swedish Research Council for Engineering Science (TFR).

Supplementary Material Available: Data tables for the experimentally obtained phase diagrams (16 pages). Ordering information is given on any current masthead page.

References and Notes

(1) Flory, P. J. *Principles of Polymer Chemistry*; Cornell University Press: Ithaca, NY, 1953.
(2) Albertsson, P.-Å. *Partition of Cell Particles and Macromolecules*; Wiley & Sons: New York, 1986.
(3) Hsu, C. C.; Prausnitz, J. M. *Macromolecules* **1974**, *7*, 320.
(4) Zeman, L.; Patterson, D. *Macromolecules* **1972**, *5*, 513.
(5) Patterson, D. *Polym. Eng. Sci.* **1982**, *22*, 64.
(6) Malcolm, G. N.; Rowlinson, J. S. *Trans. Faraday Soc.* **1957**, *53*, 921.
(7) Lindman, B.; Carlsson, A.; Karlström, G.; Malmsten, M. *Adv. Colloid Interface Sci.* **1990**, *32*, 183.
(8) Kjellander, R.; Florin, E. *J. Chem. Soc., Faraday Trans. 1* **1981**, *77*, 2053.
(9) Kjellander, R. *J. Chem. Soc., Faraday Trans. 2* **1982**, *78*, 2025.
(10) Lang, J. C.; Morgan, R. D. *J. Chem. Phys.* **1980**, *73*, 5849.
(11) Goldstein, R. E. *J. Chem. Phys.* **1984**, *80*, 5340.
(12) Karlström, G. *J. Phys. Chem.* **1985**, *89*, 4962.
(13) Andersson, M.; Karlström, G. *J. Phys. Chem.* **1985**, *89*, 4957.
(14) Björling, M.; Karlström, G.; Linse, P. *J. Phys. Chem.* **1991**, *95*, 6706.
(15) Linse, P.; Björling, M. *Macromolecules* **1991**, *24*, 6700.
(16) Sjöberg, Å.; Karlström, G. *Macromolecules* **1989**, *22*, 1325.
(17) Linse, P.; Malmsten, M. *Macromolecules* **1992**, *25*, 5434.
(18) Tiberg, F.; Malmsten, M.; Linse, P.; Lindman, B. *Langmuir* **1991**, *7*, 2723.
(19) Malmsten, M.; Linse, P.; Cosgrove, T. *Macromolecules* **1992**, *25*, 2474.
(20) Carlsson, M.; Linse, P.; Tjerneld, F. *Macromolecules*, in press.
(21) Saeki, S.; Kuwahara, N.; Nakata, M.; Kanenko, M. *Polymer* **1976**, *17*, 685.
(22) Scott, R. *J. Chem. Phys.* **1949**, *17*, 279.
(23) Björling, M.; Linse, P.; Karlström, G. *J. Phys. Chem.* **1990**, *94*, 471.
(24) Hugelin, C.; Dondos, A. *Makromol. Chem.* **1969**, *126*, 206.
(25) Kern, R. J. *J. Polym. Sci.* **1956**, *21*, 19.
(26) Bank, M.; Leffingwell, J.; Thies, C. *Macromolecules* **1971**, *4*, 43.
(27) Koningsveld, R.; Chermin, H. A. G.; Gordon, M. *Proc. R. Soc. London* **1970**, *319*. 331.
(28) Robard, A.; Patterson, D.; Delmas, G. *Macromolecules* **1977**, *10*, 706.
(29) Robard, A.; Patterson, D. *Macromolecules* **1977**, *10*, 1021.
(30) Wormuth, K. R. *Langmuir* **1991**, *7*, 1622.